Journal of Electrostatics 67 (2009) 99–104

Contents lists available at ScienceDirect

Journal of Electrostatics

journal homepage: www.elsevier.com/locate/elstat

Electrohydrodynamic flow and particle collection efficiency of a spike-plate type electrostatic precipitator

J. Podliński [a,*], A. Niewulis [a], J. Mizeraczyk [a,b]

[a] Centre for Plasma and Laser Engineering, The Szewalski Institute of Fluid Flow Machinery, Polish Academy of Sciences, Fiszera 14, 80-952 Gdańsk, Poland
[b] Department of Marine Electronics, Gdynia Maritime University, Morska 81-87, 81-225 Gdynia, Poland

ARTICLE INFO

Article history:
Received 24 September 2008
Received in revised form
28 January 2009
Accepted 9 February 2009
Available online 24 February 2009

Keywords:
Electrostatic precipitator
Electrohydrodynamic flow
Particle image velocimetry
Particle collection efficiency

ABSTRACT

In this work, the results of electrohydrodynamic (EHD) secondary flow and particle collection efficiency measurements in a spike-plate type electrostatic precipitator (ESP) are presented. The EHD secondary flow was measured using 2- and 3-dimensional particle image velocimetry (PIV) method under the negative DC voltage. The PIV measurements were carried out in several cross-sectional planes along and across the ESP duct. The results show a complex and turbulent flow structure in the ESP. The EHD secondary flow significantly depends on applied voltage and measuring cross-sectional plane position in respect to the spike tip. The partial collection efficiency of the ESP was measured for negative and positive DC voltage. The particle concentration with and without discharge was measured at the ESP exit using an optical aerosol spectrometer.

1. Introduction

For several decades electrostatic precipitators (ESPs) have been widely used as dust particle collectors since ESPs have relatively high particle collection efficiency (up to 99.9%) with a relatively low pressure drop. However, the collection efficiency of sub-micron dust particles (of a size typically ranging from 0.1 μm to 1 μm) is relatively lower [1,2] (sometimes less than 50%) due to the mismatching of particle charging and migration velocity.

Sub-micron dust particles which may contain rich toxic trace elements, float for relatively long time in the atmosphere and can easily penetrate into human respiratory system. Therefore, new standards for emission of fine particles are introduced (PM2.5). The existing ESPs have to be modified to meet new standards.

The motion and precipitation of particles in the duct of an ESP depend on the dust particle properties, electrode geometry, electric field, space charge and gas flow field [3]. It has been shown [4–6] that a significant interaction between these factors exists, resulting in considerable turbulent flow structures in the volume between stressed and collecting electrodes. There are evidences which show that the flow turbulences can influence the collection efficiency of fine particles [7,8].

One of the methods to improve the particle collection efficiency in ESPs is to use a spiked discharge electrode [9–11]. However, there were no comprehensive investigations on the electrohydrodynamic (EHD) secondary flow field in ESPs with spike discharge electrode.

This work was aimed at measuring EHD secondary flow in a spike-plate ESP using 2- and 3-dimensional particle image velocimetry (PIV) [12]. Also the particle collection efficiency of the ESP was measured in similar conditions.

2. Experimental set-up

The apparatus used in this experiment to EHD secondary flow measurements consisted of an ESP, a high-voltage supply, and a standard PIV equipment for the measurement of velocity fields (Fig. 1).

The ESP housing used in this work was an acrylic box, 1000 mm long, 200 mm wide and 100 mm high. At the top and bottom of the ESP housing two collecting stainless-steel plate electrodes (200 mm × 600 mm) were placed. In the middle of the ESP the spike electrode (200 mm long, 1 mm thick, and 30 mm tip-to-tip wide) was mounted in the acrylic side walls, parallel to the plate electrodes and perpendicularly to the main flow (Fig. 2). The spike tips were directed upstream on the one side of the electrode, and downstream on the other. The distance from the spike electrode to the plate electrodes was 50 mm.

The negative voltage applied to the spike electrode was up to 27.4 kV, and the time averaged discharge current was up to 260 μA.

* Corresponding author. Tel.: +48 58 6995122; fax: +48 58 3416144.
E-mail address: janusz@imp.gda.pl (J. Podliński).

0304-3886/$ – see front matter © 2009 Elsevier B.V. All rights reserved.
doi:10.1016/j.elstat.2009.02.009

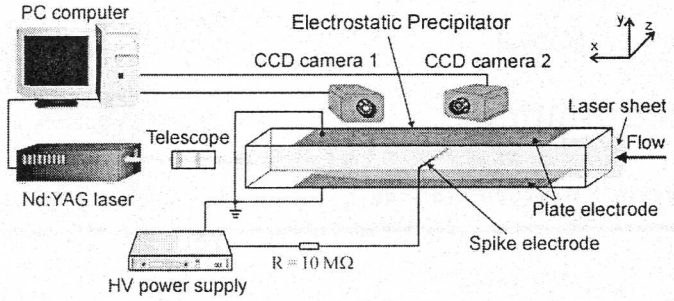

Fig. 1. Experimental set-up for PIV flow velocity field measurements in the ESP.

The voltage was supplied to the spike electrode through a 10 MΩ resistor. Air flow seeded with a fine TiO_2 particles (size of less than 1 μm) was blown along the ESP duct with an average velocity of 0.6 m/s.

The PIV measurements were carried out in eight different cross-sectional planes (planes A–H, see Fig. 2), all placed perpendicularly to the plate electrodes. Three planes (A, B and C) were fixed along the ESP housing. The first of them (plane A) passed through the tip of the upstream-directed central spike electrode, the second plane (plane B) passed in-between the upstream and downstream spikes, while the third plane (plane C) passed through the tip of the neighbouring downstream-directed spike electrode. Planes D–H were spaced equally across the ESP housing, from 60 mm upstream the spike electrode ($x = -60$ mm) to 60 mm downstream the spike electrode ($x = 60$ mm).

The flow velocity field maps (area of 260 mm × 100 mm) obtained in planes A, B and C were composed of three adjacent overlapping velocity fields (area of each 100 mm × 100 mm). All presented velocity fields resulted from the averaging of 100 measurements, which means that each velocity map was time averaged. Based on the averaged velocity fields, the flow streamlines were calculated.

The study of fine particles collection was carried out in the same spike-plate type ESP. During these measurements air flow seeded with a cigarette smoke (cigarettes trademark: Popularne) was blown along the ESP section with an average velocity of 0.6 m/s. In order to prevent fluctuations in the mean concentration of the cigarette smoke particles, a set-up based on the balloon of about

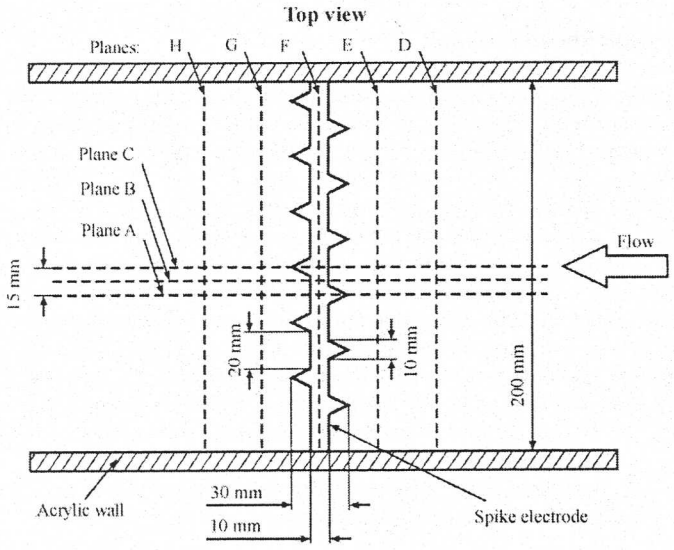

Fig. 2. Top-view schematic drawing of the spike-plate ESP.

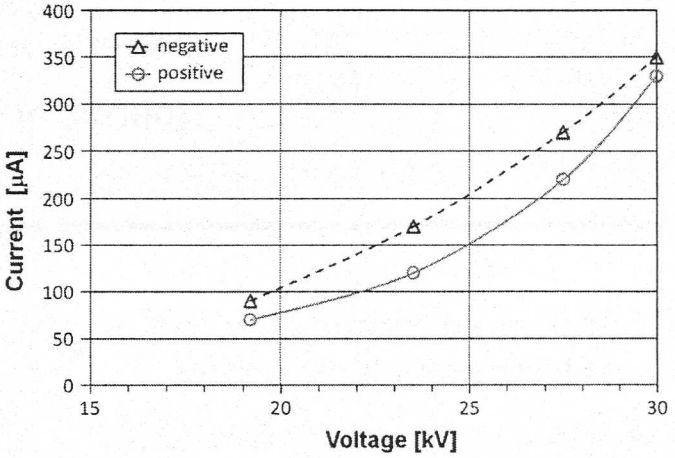

Fig. 3. Time averaged current–voltage characteristics of the discharge in spike-plate type ESP for positive and negative voltage polarities.

2 m in diameter (volume of about 4 m^3) for forming the suspension was introduced into the gas duct. At the ESP exit a turbulence mixer was placed in the gas duct. For the particle concentration measurements the suspension was sucked behind turbulence mixer. The measurements were carried out for positive and negative applied voltage, directly one after another and in similar conditions (temperature 17 °C and relative humidity 45%). The measured time averaged current–voltage characteristics are shown in Fig. 3.

The measurement of the particle concentrations by classes of size was carried out using an optical aerosol spectrometer (GRIMM 1.109) (particle size scales ranging from 0.25 μm to 32 μm). The counting of particles was performed at the ESP exit with and without applied voltage. For a size class of particles characterized by a diameter d_p, the partial efficiency of collection $\eta_f(d_p)$ was determined by:

$$\eta_f(d_p) = 1 - \frac{c_{HV}(d_p)}{c_0(d_p)},$$

where $c_{HV}(d_p)$ and $c_0(d_p)$ are the particle concentrations measured behind the ESP and turbulence mixer, with high voltage applied and without voltage, respectively. In order to reduce the statistical fluctuations, the counting of particles was performed during a cumulated time of 2 min for $c_{HV}(d_p)$ and 2 min for $c_0(d_p)$.

3. Results

Figs. 4–12 show results obtained in the spike-plate ESP at a primary flow average velocity of 0.6 m/s. At this velocity the

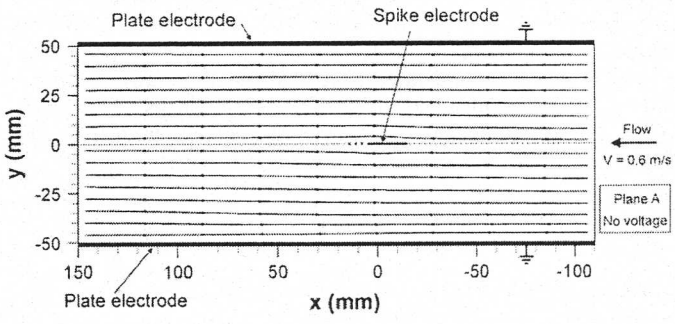

Fig. 4. Averaged flow streamlines measured in the plane A in the spike-plate type ESP when no voltage was applied.

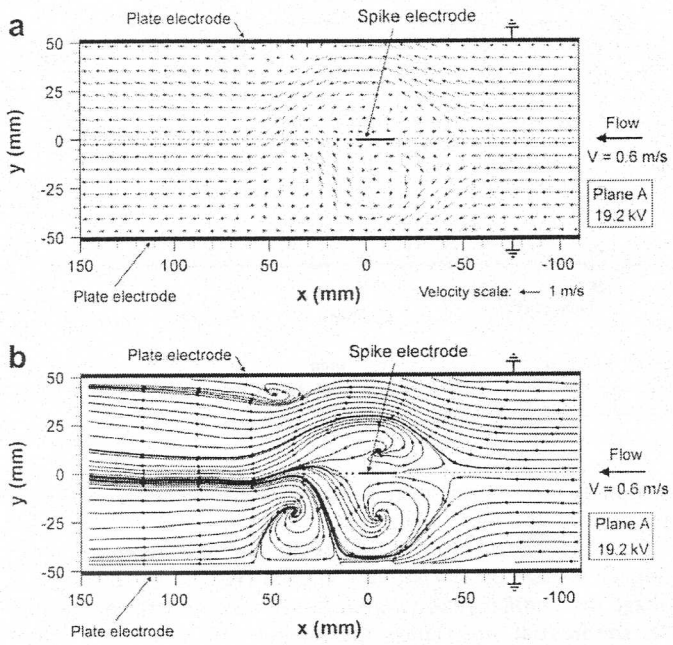

Fig. 5. Averaged flow velocity field (a) and corresponding flow streamlines (b) measured in the plane A in the spike-plate ESP. Negative voltage of 19.2 kV was applied, discharge current was 80 μA. Ehd was 2.5×10^7 and Ehd/Re^2 was 1.7.

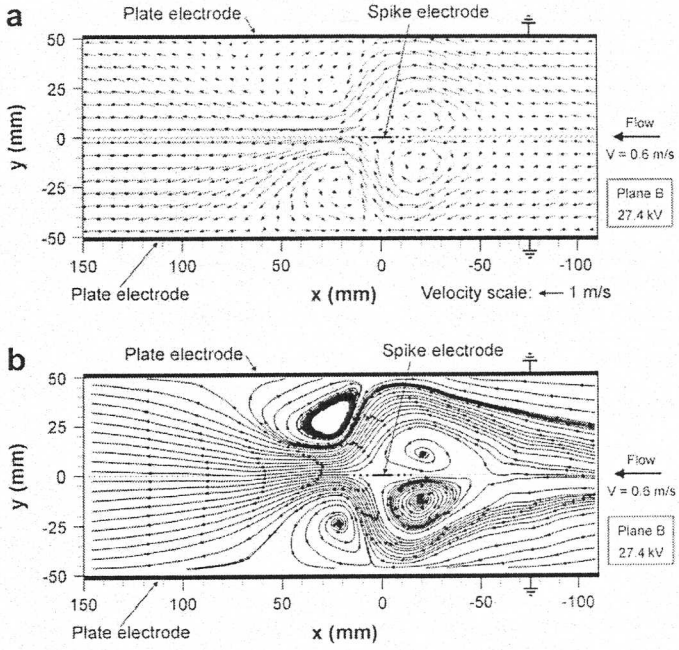

Fig. 7. Averaged flow velocity field (a) and corresponding flow streamlines (b) measured in the plane B in the spike-plate ESP. Negative voltage of 27.4 kV was applied, discharge current was 260 μA. Ehd was 8.1×10^7 and Ehd/Re^2 was 5.6.

Reynolds number was $Re = V \times L/\nu = 3800$ (the parameters used to calculate Re were: the primary flow velocity $V = 0.6$ m/s, characteristic length (plate-plate distance) $L = 0.1$ m, and air kinematic viscosity $\nu = 1.57 \times 10^{-5}$ m^2/s).

When no voltage was applied, the measured flow velocity fields and corresponding flow streamlines (Fig. 4) show that the flow in the ESP was laminar (corresponding to the transition region for $Re > 2300$). Small wake flow around the spike electrode was observed.

When a high voltage was applied, the electric force exerted by the corona discharge and electric field induces a considerable EHD secondary flow which altered significantly the primary laminar flow. The flow patterns in the ESP changed significantly, depending on applied voltage. Figs. 5–12 show results for applied voltages of 19.2 kV and 27.4 kV. The time averaged discharge current was 80 μA and 260 μA, respectively. Thus the corresponding electrohydrodynamic numbers [Ehd $= I \times L^3/(\nu^2 \times \rho \times \mu_i \times A)$] [13], based on the flow channel data, were 2.5×10^7 and 8.1×10^7. Hence, the

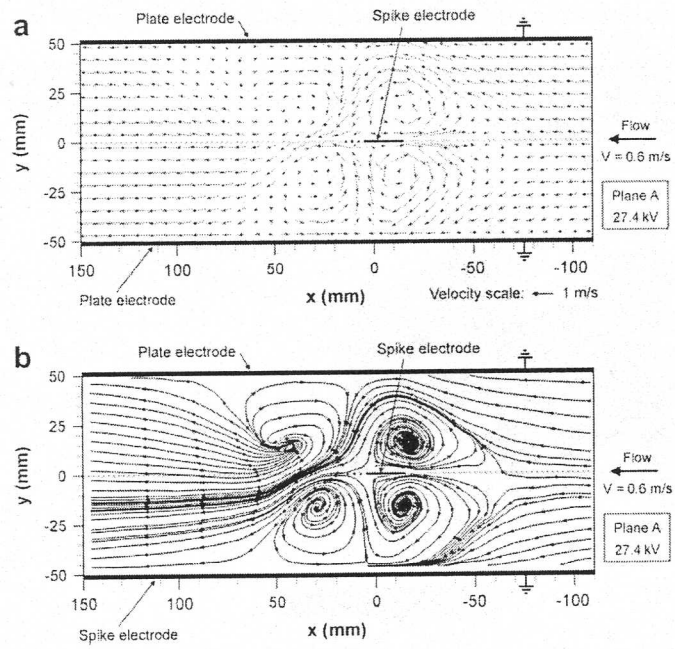

Fig. 6. Averaged flow velocity field (a) and corresponding flow streamlines (b) measured in the plane A in the spike-plate ESP. Negative voltage of 27.4 kV was applied, discharge current was 260 μA. Ehd was 8.1×10^7 and Ehd/Re^2 was 5.6.

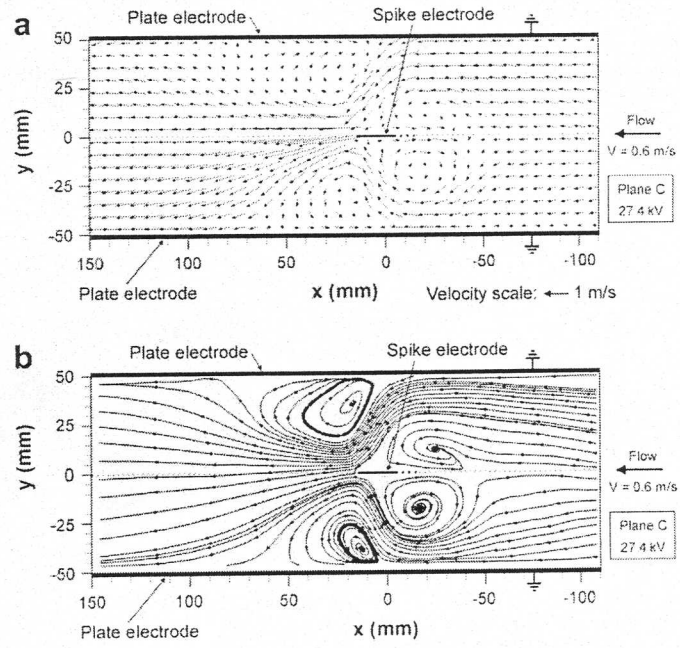

Fig. 8. Averaged flow velocity field (a) and corresponding flow streamlines (b) measured in the plane C in the spike-plate ESP. Negative voltage of 27.4 kV was applied, discharge current was 260 μA. Ehd was 8.1×10^7 and Ehd/Re^2 was 5.6.

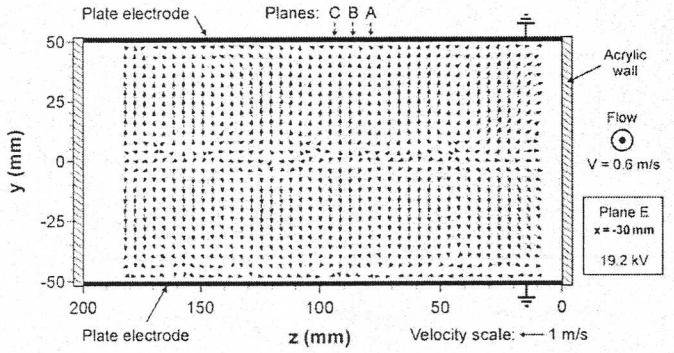

Fig. 9. Averaged flow velocity field measured in the plane E in the spike-plate ESP. Negative voltage of 19.2 kV was applied, discharge current was 80 μA. Ehd was 2.5×10^7 and Ehd/Re^2 was 1.7.

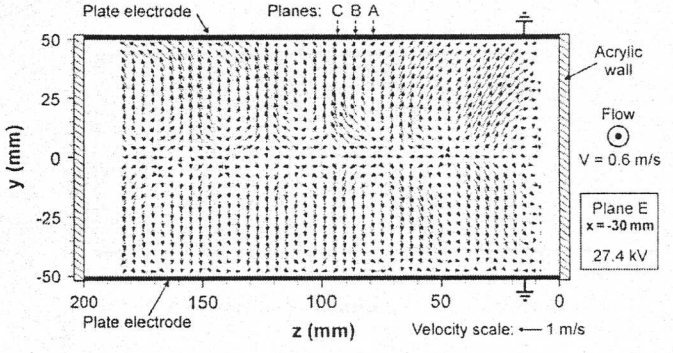

Fig. 10. Averaged flow velocity field measured in the plane E in the spike-plate ESP. Negative voltage of 27.4 kV was applied, discharge current was 260 μA. Ehd was 8.1×10^7 and Ehd/Re^2 was 5.6.

ratios of the EHD number to the Reynolds number squared (Ehd/Re^2 describes the ratio of the electric forces to the inertial force) were 1.7 (for 19.2 kV) and 5.6 (for 27.4 kV). The parameters used to calculate Ehd were: the total discharge current I, characteristic length (plate–plate distance) $L = 0.1$ m, air kinematic viscosity $\nu = 1.57 \times 10^{-5}$ m^2/s, air density $\rho = 1.205$ kg/m^3, ion mobility $\mu_i = 2.7 \times 10^{-4}$ m^2/V s, and discharge area (100 mm long and 200 mm wide discharge area on the two plate electrodes) $A = 2 \times 100$ mm $\times$ 200 mm $= 0.04$ m^2. The uniform current distribution on the plate electrodes was assumed. This assumption was justified by the optical emission intensity measurements of the discharge from the spike electrode (observation of N_2 Second Positive Band emission which is proportional to the electron density [10]).

Fig. 5 shows results of the PIV measurements in the plane A, when a high voltage of 19.2 kV was applied. As can be seen, two pairs of vortices occurred. One pair developed near the upstream-directed spike tip, and the second one in the downstream of the spike electrode and near the plate electrodes. The pair of vortices near the upstream-directed spike tip blocks the primary flow in the central part of the ESP housing and causes the flow to move nearer both plate electrodes. In the downstream of the spike electrode, the vortices do not allow the main flow to move near the plate electrodes. As a result, after passing the spike electrode the main flow turns towards the ESP centre and passes between the downstream vortices. For both vortex pairs there are quite considerable differences in sizes and strength of the vortices. This is probably due to asymmetry of the primary flow profile at the ESP inlet (it can be seen at $x = -100$ mm, in Fig. 5a).

The vortex structures were much more symmetrical when a higher voltage of 27.4 kV was applied (Fig. 6). At such a high voltage the Ehd/Re^2 ratio was 5.6, so the electric force dominates over the inertial one. Hence, the influence of asymmetry of the primary flow profile at the ESP inlet was weaker. The vortices near the upstream-directed spike tip and in the downstream of the spike electrode became stronger and occupied almost the whole ESP height.

The flow velocity field and corresponding flow streamlines measured in the plane B when a high voltage of 27.4 kV was applied are presented in Fig. 7. Two pairs of vortices, upstream and downstream of the spike electrode, developed also in the plane B (fixed in the midway between the upstream- and downstream-directed spike tips, see Fig. 2). However, the vortices in this plane are smaller than those in the plane A of the same voltage.

The EHD flow patterns in the plane C (Fig. 8), passing through the downstream-directed spike tip (Fig. 2), were similar to those observed in the plane B. The vortex structures close to the spike electrode and near the plate electrodes were present. However, these vortices did not cover the whole ESP height, and a considerable part of the primary flow moved between vortices and then to the ESP exit.

Comparing the EHD secondary flow measured in the spike-plate type ESP one can deduce that the stronger vortices occur at higher Ehd/Re^2 ratio (Figs. 5 and 6). However, the strength and dimension

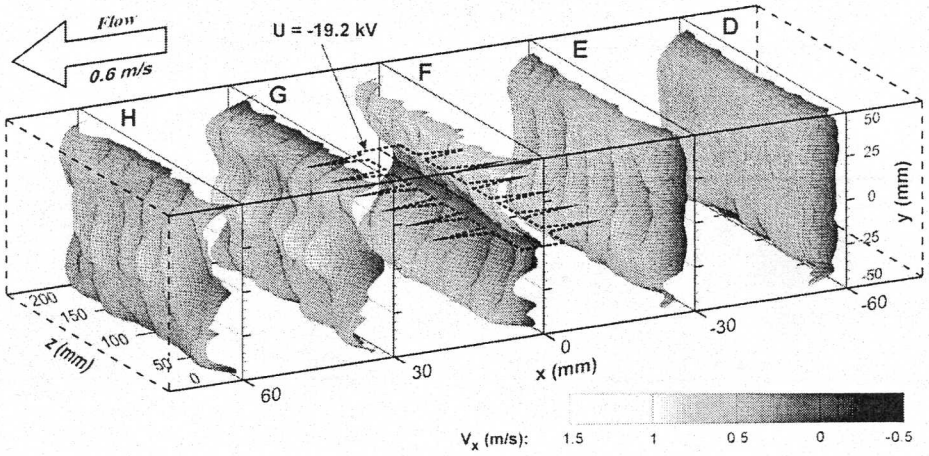

Fig. 11. Averaged flow velocity x-component measured in planes D–H in the spike-plate ESP. Negative voltage of 19.2 kV was applied, discharge current was 80 μA. Ehd was 2.5×10^7 and Ehd/Re^2 was 1.7.

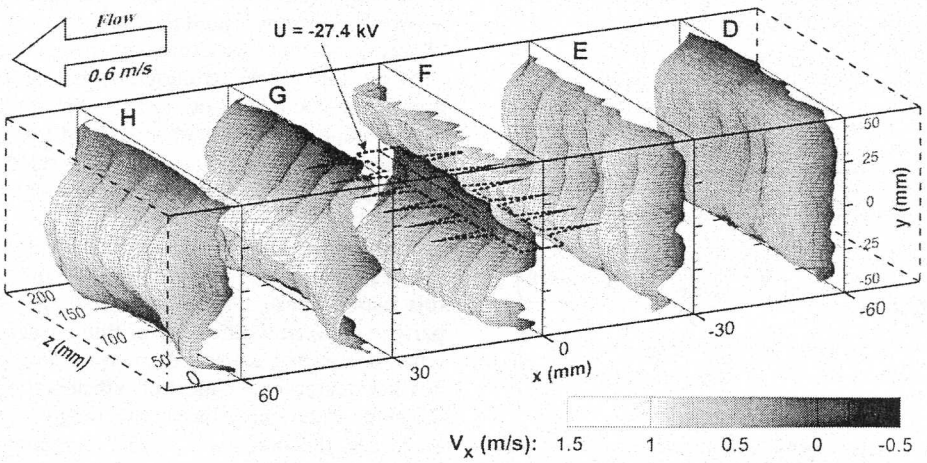

Fig. 12. Averaged flow velocity x-component measured in planes D–H in the spike-plate ESP. Negative voltage of 27.4 kV was applied, discharge current was 260 μA. Ehd was 8.1×10^7 and Ehd/Re^2 was 5.6.

of the vortices depend also on the directions of the EHD secondary flow and the primary flow in respect to each other. The vortices in the plane A are stronger than in the plane C, although the Ehd/Re^2 ratio in the planes A and C is the same. This difference is a result of a strong interaction of the upstream-directed EHD secondary flow from the upstream spike tip in the plane A with the oppositely directed primary flow. This strong interaction causes the strong vortices observed in the plane A. On the other hand, in the plane C the directions of the EHD secondary flow and the primary flow are in accordance. Therefore, their interaction is weaker and vortices in the plane C are not significant.

Analyzing the two-dimensional flow patterns presented in Figs. 6–8, it can be deduced that the flow in the presented spike-plate ESP is three-dimensional, similarly as in the wire-plate type ESP under negative polarity due to tuft corona spots [14]. The complex three-dimensional nature of the flow pattern in the spike-plate type ESP was confirmed by 3D PIV measurements (Figs. 9–12), carried out in planes D–H (planes perpendicular to the primary flow direction).

Figs. 9 and 10 show that the flow velocities in y- and z-directions (perpendicular to the primary flow direction) measured in the plane E are considerable. When 19.2 kV was applied (Fig. 9), the velocity y-component reaches values up to 0.3 m/s while the velocity z-component was up to 0.15 m/s in the vicinity of the central spike tips and even higher than 0.3 m/s in the vicinity of the acrylic side walls. For applied voltage of 27.4 kV (Fig. 10) these velocity components are even higher, the velocity y-component reaches values up to 0.7 m/s while the velocity z-component was up to 0.5 m/s in the ESP centre and up to 0.7 m/s near the side walls. The side walls considerably disturb the flow around the nearest spike tips. However, the flow patterns around the central spike tips are stable and very similar to each other.

The flow velocity x-component (in the primary flow direction) measured in planes D–H in the ESP, for negative voltage of 19.2 kV, is shown in Fig. 11. In the plane D (placed at $x = -60$ mm), the velocity profile is not much disturbed. The velocity x-component is about 0.7 m/s in the volume of the ESP duct and clearly decreases near the side walls and plate electrodes (in the boundary layers). In the planes E–H quite regular flow structures, originated from the spike tips, occurred. The velocity x-component reaches values from 0.3 m/s in the opposite direction to the primary flow direction (in the plane E, in the area before the upstream-directed spike tips) to 1 m/s in the primary flow direction (in the plane G, in the area behind the downstream-directed spike tips). When negative voltage of 27.4 kV was applied (Fig. 12) the velocity profile was disturbed much more than for the lower voltage. Some flow disturbances in the central part of the ESP duct were found in the plane D. The characteristic flow structures, originated from the spike tips, also occurred in the planes E–H. They were stronger than at the lower voltage (19.2 kV). The velocity x-component reaches

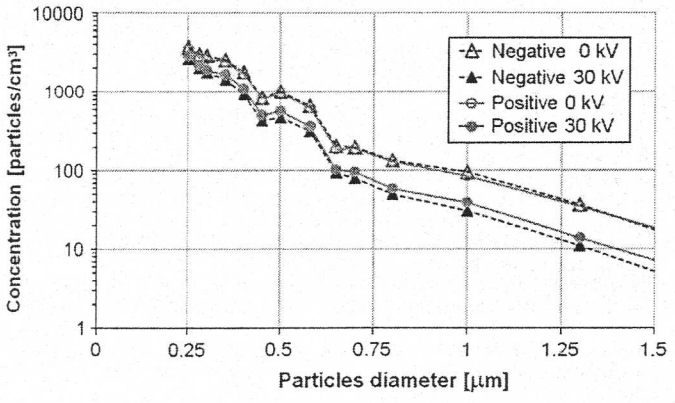

Fig. 13. Particle density (in particles/cm^3) of cigarette smoke particles with and without voltage (positive or negative) of 30 kV measured at the spike-plate type ESP exit.

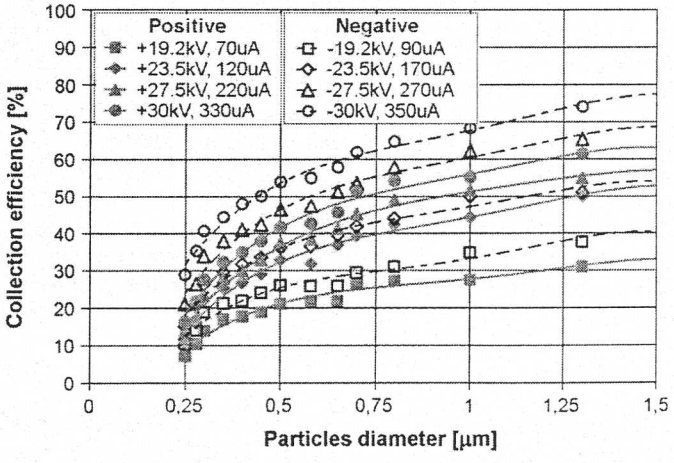

Fig. 14. Partial collection efficiency versus particle diameter for various applied voltage (positive or negative) as measured at the spike-plate type ESP exit.

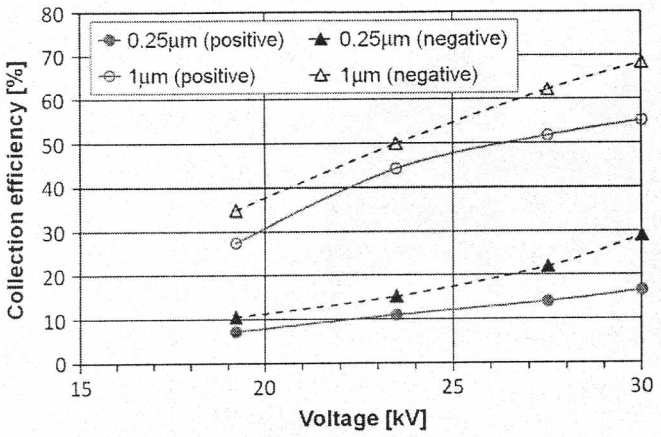

Fig. 15. Partial collection efficiency versus applied voltage (positive or negative) for particles diameter of 0.25 μm and 1 μm as measured at the spike-plate type ESP exit.

values from 0.5 m/s in the opposite direction to the primary flow direction and up to 1.5 m/s in the primary flow direction.

Typical size distributions of cigarette smoke particles obtained for 0 kV and 30 kV are shown in Fig. 13. The particle number density distributions clearly show that the majority of particles are sub-micron particles of a diameter 0.25 μm. Approximately 99% of particles were of diameters below 1 μm. For −30 kV of applied voltage 99.5% of particles had a diameter below 1 μm.

The partial particle collection efficiency η_f as a function of particle diameter d_p is shown in Fig. 14 for 19.2 kV, 23.5 kV, 27.5 kV and 30 kV for both voltage polarities. Fig. 14 shows that the collection efficiency η_f increases with increasing applied voltage, as expected. The negative voltage polarity is more efficient in the particle collection than the positive one, as met in the commercial ESPs [1,2]. For the both applied voltage polarities, the collection efficiency decreases when particles' diameter decreases. This tendency is most distinct for sub-micron particles in the range 0.25–0.5 μm, as expected from the dependence mismatch between charging-particle diameter and charged-particle migration velocity [1,2]. Here, we must note that the partial particle collection efficiency usually exhibits a minimum for particle size between 0.2 μm and 0.5 μm in the majority of ESPs [1,2]. Therefore, even for negative voltage of −30 kV (most efficient studied case) the measured collection efficiency of fine particles (diameter of 0.25 μm) was below 30%.

The collection efficiency η_f as a function of applied voltage for two size classes of particles is presented in Fig. 15. It is clearly seen from this figure that the collection efficiency of the ESP with negative voltage is higher than for positive one. The higher collection efficiency of the negative polarity could be explained by a higher discharge current (due to higher ion mobility and resulting higher charged-particle density) for the same voltage (see Fig. 3). However, one should notice that the collection efficiency η_f for a positive voltage of 30 kV and a discharge current of 280 μA was even lower than the collection efficiency for a negative voltage of 27.5 kV and a discharge current of 260 μA. This might indicate that the vortex-type negative voltage EHD secondary flow with longer particle residence time in the ESP may enhance the collection efficiency.

4. Conclusion

In this paper results of the 2-D and 3-D PIV measurements of the flow velocity fields in several planes along and across the negatively polarized ESP are presented. The obtained results showed very complicated flow patterns in the spike-plate ESP with characteristic flow structures for the spike tips. We found that the EHD secondary flow strongly depends on the applied voltage and measuring plane position in respect to the spike tip. The strongest vortices appeared for higher applied voltage (i.e. for higher Ehd number) and in the plane passing through the upstream-directed spike tip (plane A). The flow in the spike-plate ESP is strongly three-dimensional.

The partial particle collection efficiency of the spike-plate ESP for negative and positive voltage polarity was also presented in this paper. These results confirmed the common view that the particle collection efficiency of fine particles in the ESP decreases when decreasing particle diameter and applied voltage. The most distinct decrease of collection efficiency with decreasing particle diameter is for particles in the range from 0.25 μm to 0.5 μm. Moreover, the presented results suggest that the collection efficiency of the spike-plate type ESP with negative voltage applied was higher than for positive voltage polarity not only due to the pure electrical reasons (e.g. higher ion mobility) but also due to EHD secondary flow.

Acknowledgement

Authors are very grateful to J.S. Chang and P. Atten for fruitful discussions, comments and some experimental suggestions.

This work was supported by the Ministry of Science and Higher Education (grants PB 1857/B/T02/2007/33 and 3892/B/T02/2008/35).

References

[1] A. Mizuno, Electrostatic precipitation, IEEE Trans. Diel. Electr. Insul. 7 (2000) 615–624.
[2] S. Masuda, S. Hosokawa, Chapter 21 of Handbook of Electrostatic Processes, Marcel Dekker, NY, 1995, pp. 441–479.
[3] P. Atten, F.M.J. McCluskey, A.C. Lahjomri, The electrohydrodynamic origin of turbulence in electrostatic precipitators, IEEE Trans. Ind. Appl. 23 (1987) 705–711.
[4] T. Yamamoto, H.R. Velkoff, Electrodynamics in an electrostatic precipitator, J. Fluid Mech. 108 (1981) 1.
[5] W.J. Liang, T.H. Lin, The characteristics of ionic wind and its effect on electrostatic precipitators, Aerosol Sci. Technol. 20 (1994) 330.
[6] J. Podliński, A. Niewulis, J. Mizeraczyk, P. Atten, ESP performance for various dust densities, J. Electrostat. 66 (2008) 246–253.
[7] U. Kogelschatz, W. Egli, E.A. Gerteisen, Advanced computational tools for electrostatic precipitators, ABB Rev. 4 (1999) 33–42.
[8] P. Atten, H.L. Pang, J.L. Reboud, J. Podliński, J. Mizeraczyk, Turbulence generation by charged fine particles in electrostatic precipitators, in: Proc. ESA Annual Meeting on Electrostatics 2007, Laplacian Press, 2007, pp. 259–270.
[9] D. Brocilo, J.S. Chang, R.D. Findlay, Y. Kawada, T. Ito, Modelling of the effect of electrode geometries on the corona discharge current–voltage characteristic for wire-plate electrostatic precipitators, 2001 Annual Report Conference on Electrical Insulation and Dielectric phenomena, pp. 681–684.
[10] D. Brocilo, J.S. Chang, R.D. Findlay, Modeling of electrode geometry effects on dust collection efficiency of wire-plate electrostatic precipitators, in: Proceedings of 8th International Conference on Electrostatic Precipitation, vol. I, 2001, pp. 1–18.
[11] J. Podliński, J. Dekowski, J. Mizeraczyk, D. Brocilo, K. Urashima, J.S. Chang, EHD flow in a wide electrode spacing spike-plate electrostatic precipitator under positive polarity, J. Electrostat. 64 (2006) 498–505.
[12] M. Raffel, Ch.E. Willert, J. Kompenhans, Particle Image Velocimetry, A Practical Guide, Springer-Verlag, Berlin, Heidelberg, 2007.
[13] IEEE-DEIS-EHD Technical Committee, Recommended international standard for dimensionless parameters used in electrohydrodynamics, IEEE Trans. Diel. Electr. Insul. 10 (1) (2003) 3–6.
[14] Y. Yamamoto, M. Okuda, M. Okubo, Three-dimensional ionic wind and electrohydrodynamics of tuft/point corona electrostatic precipitator, IEEE Trans. Ind. Appl. 39 (2002) 1602–1607.